Pragmatic Image Reconstruction for the MiCES Fully-3D Mouse Imaging PET Scanner

Kisung Lee, *Student Member, IEEE,* Paul E. Kinahan, *Senior Member, IEEE*, Jeffrey A. Fessler, *Senior member, IEEE*, Robert S. Miyaoka, *Member, IEEE*, and Tom K. Lewellen, *Member, IEEE*

***Abstract*-- We present a pragmatic approach to image reconstruction for data from the MiCES fully-3D mouse imaging PET scanner under construction at the University of Washington. Our approach is modeled on fully-3D image reconstruction used in clinical PET scanners, which is based on Fourier rebinning (FORE) followed by 2D iterative image reconstruction. The use of iterative methods allows modeling the effects of statistical noise and attenuation etc., while FORE accelerates the reconstruction process by reducing the fully-3D data to a stacked set of independent 2D sinograms. Preliminary investigations have indicated that non-stationary detector point-spread response effects, which are ignored for clinical imaging, significantly impact image quality for the MiCES scanner geometry. To model the effect of non-stationary detector point spread response, we have added a factorized system matrix to the ASPIRE reconstruction library. The current implementation uses FORE+AWOSEM followed by post-reconstruction 3D Gaussian smoothing. The results indicate that the proposed approach produces a dramatic improvement in resolution without undue increases in noise.**

I. Introduction

In this paper we present the initial results of a 'pragmatic' approach to image reconstruction for data from the MiCES fully-3D mouse imaging PET scanner [1] under construction at the University of Washington. Our approach is modeled on fully-3D image reconstruction used in clinical PET scanners, which is based on Fourier rebinning (FORE) [2] followed by 2D iterative image reconstruction.

The limiting factor in image quality for many PET studies are the high levels of statistical noise. This is potentially even more of an issue for imaging studies of mice, as only small volumes (typically 100 μl or less) of radio-labeled tracers can be injected due to the small blood volume of mice (typically on the order of 20 ml).

One method of reducing statistical noise is by increasing the sensitivity of the scanner. This can be done by operating the scanner in a fully-3D acquisition mode. This acquisition mode increases the sensitivity by a factor of approximately five- to ten-fold, but increases the computational demands for data storage and image reconstruction.

This work was supported by NIH grants CA-74135, CA-86892, and EB0217.

An alternate method of reducing statistical noise in the reconstructed image is to use a model of the Poisson-distributed imaging statistics in the reconstruction algorithm. In this case, however, the resulting set of equations describing the forward-problem becomes very large and non-linear, and solving for the tracer distribution by direct inversion of the forward-problem becomes intractable. In this case the equations must be solved using iterative methods.

The use of FORE accelerates the reconstruction process by converting the fully-3D sinograms to a stack of 2D sinograms. This reduces the sinogram data size and image reconstruction problem by at least an order of magnitude, but also introduces some degradation of the image SNR characteristics compared to a fully-3D reconstruction.

The use of iterative methods allows modeling the effects of statistical noise and attenuation, etc. Our preliminary investigations [3] indicated that non-stationary detector point-spread response effects, which are ignored for clinical imaging, significantly impact image quality for the MiCES scanner geometry.

Several methods of image reconstruction for small animal PET scanners have been published [8], [9], [12], [14]. Among those works, the studies by Qi and Leahy et al. in [8] and [9] proposed a method with factorization of the system matrix that consists of independent matrices representing corresponding to sequential physical effects that occur in the data stream of a PET scanner. By doing the factorization and matrix computation 'on the fly', their method can produce high resolution images but at a high computational cost caused by very large size of the fully-3D system matrix.

To model the effects of positron range and non-stationary detector point-spread response, we have added a factorized system matrix to the ASPIRE [4]-[6] reconstruction library. We also include the first-order effect of FORE rebinning on sinogram variance. The current implementation uses FORE+AWOSEM [7] followed by post-reconstruction 3D Gaussian smoothing. The use of the ASPIRE library, however, allows for potential utilization of more sophisticated algorithms with proven convergence.

The proposed approach was used to reconstruct simulated data and measured data from single-ring MiCES evaluation system [11] under development at the University of Washington. Those results were also compared with the

0-7803-8257-9/04/$20.00 © 2004 IEEE.

techniques (FORE+FBP and FORE+OSEM) used in existing clinical imaging.

II. Simulation Studies

A. The MiCES scanner and a simplified model

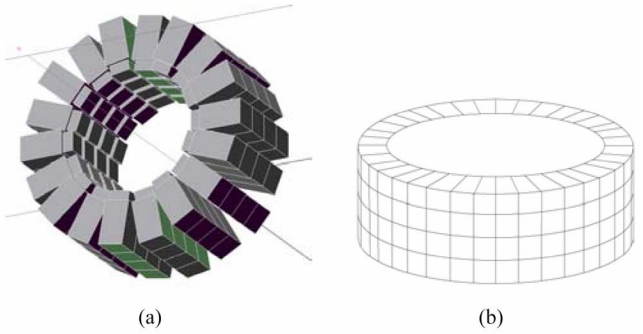

(a) (b)

Fig. 1. (a) Detector module arrangement for the MiCES scanner, (b) simplified model of (a) for the simulation model

The full MiCES machine will consist of 4 rings (12 cm diameter) of modules, with each ring comprised of 18 position sensitive photomultiplier tube (PMT) blocks, see Fig.1 (a). The scanner utilizes a total of 72 photo multiplier tubes (PMTs) (18 blocks x 4 rings), each coupled to a 22 x 22 array of 0.8 x 0.8 x 10 mm discrete mixed lutetium silicate (MLS) crystals. And there is 0.1 mm inter-crystal gap between adjacent crystals. In modeling the scanner for this study, the target detector modules were simplified into Fig. 1 (b). In the simplified model, a ring was divided into 396 equally spaced discrete crystals (22 crystals x 18 blocks) along the circumference of the ring. In the axial direction, 4 rings were split into 88 crystals (22 blocks x 4 rings). Keeping the same detector ring diameter, the crystal cross-sections were 1x1 mm^2. No gap was considered between adjacent crystals and the length of the crystals was 10 mm.

B. Detector point spread function generation

Spatially-varying detector point-spread functions (PSFs) in projection domain were generated using SimSET for the simplified model of MiCES described in Section II.A. The method described in [3] and [13] was used to get PSFs at all bin locations. Fig. 2 shows detector PSFs at the locations of 0, 12, and 24 mm off-centered position from field of view (FOV) center. As a position of distance bin goes to FOV boundary, shape of corresponding PSF becomes wider and more asymmetrical.

C. Reconstruction with point sources

A point-sources phantom that covers most area of FOV was generated in order to investigate effects of our pragmatic approach in whole FOV. Point sources are spheres with 2 mm diameter and are located at positions with the radial distances of 0, 12, and 24 mm from the transaxial center and with 0, 10, and 20 mm axial distances from axial center of FOV. A cylindrical attenuation object with water equivalent was generated to cover whole field of view.

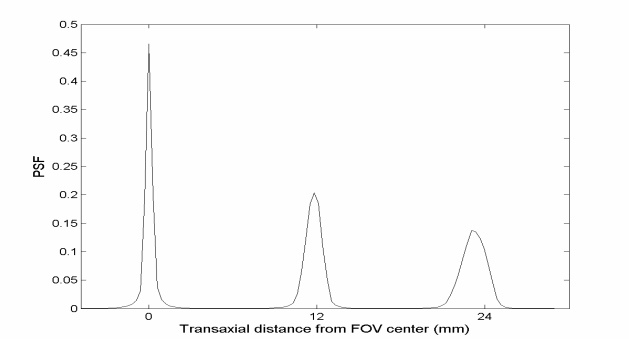

Figure 2. Detector point spread functions at FOV center, 12 and 24 mm off-centered position in projection domain

System matrix was generated based on parallel strip-integrals (system 2 in Aspire) with 0.45 mm strip width. Fig. 3 (a) is a transverse slice of SSRB+FBP images while (b)-(d) are slices for FORE+FBP, FORE+OSEM and FORE+OSEM incorporating detector blurring PSFs (FORE+OSEM_DB). As shown by Matej et al. [10], SSRB introduces severe distortions of data in both transverse and coronal planes while FORE produces data with similar quality throughout the whole FOV area. Based on the results of Fig. 3, SSRB was not explored further in this study. The results in Fig. 3 also indicate that, within the same rebinning technique, the 'pragmatic' approach, OSEM_DB, produces higher performance of resolution recovery while FBP and OSEM yield similar resolution for this test object.

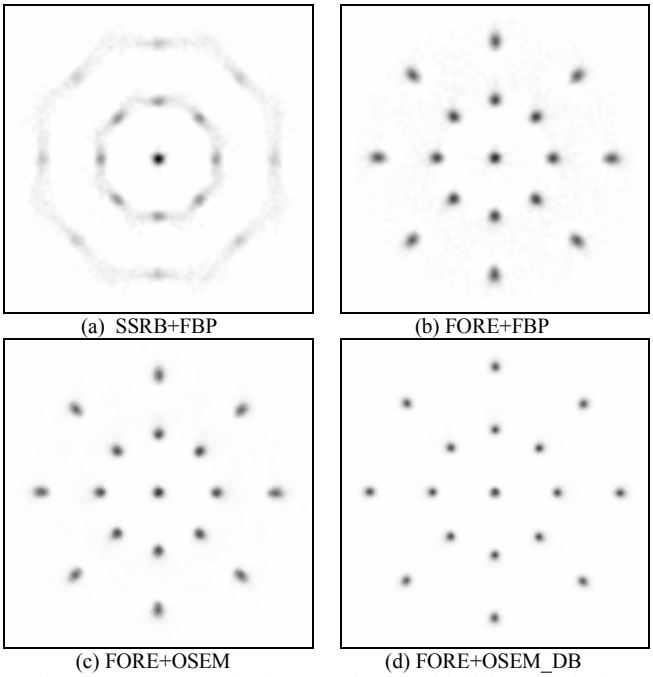

(a) SSRB+FBP (b) FORE+FBP

(c) FORE+OSEM (d) FORE+OSEM_DB

Figure 3. Reconstructed point source images with different methods.

Radial profiles taken along the transverse axis in FORE reconstruction images (Fig. 3 (b)-(d)) are shown in Fig. 4. Full-width-and-half-maximum (FWHM) values of those profiles are also displayed in Table I. Both results indicate that

OSEM_DB produces a dramatic improvement in resolution in terms of contrast and FWHM. Resolution is recovered more significantly at the FOV boundary. In addition, OSEM_DB also corrects the radial locations of point sources, which were shifted towards the center due to the blurring effects caused by parallax effects and inter-crystal scattering.

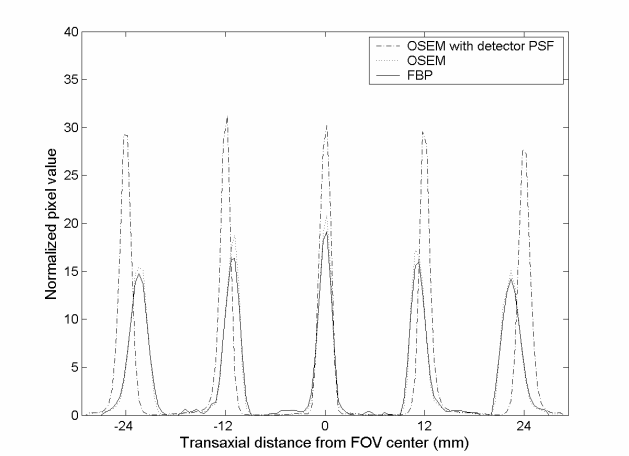

Figure 4. Radial profiles of reconstructed point sources in Fig. 3 (b)-(d)

TABLE I
FWHMS OF RECONSTRUCTED POINT SOURCES IN FIG. 4

Reconstruction method	Center (mm)	12 mm offset (mm)	24 mm offset (mm)
FBP	1.92	2.16	2.48
OSEM	1.78	2.02	2.44
OSEM_DB	1.68	1.45	1.64

III. MEASURED DATA FROM THE MICES EVALUATION SYSTEM

The proposed image reconstruction method was applied to reconstruct measured data acquired from the single ring MiCES evaluation system called QuickPET II [11] shown in Fig. 5. It has 1 ring (12.65 cm diameter) of 18 detector arrays each coupled to a position sensitive photomultiplier tube (PMT) blocks. PMT and crystal specifications are same as those described in Section II.A. The transverse FOV diameter is 5.76 cm and the axial length of the FOV is 1.98 cm.

For the target MiCES scanner with 4 rings, continuous rotation functionality will be realized for gap compensation. However, the current evaluation system provides manual rotation functionality (+/-10°) that requires a rotated normalization process among sinograms acquired at different angles.

A. Detector blurring point-spread functions

A requirement for the proposed reconstruction approach is to measure the spatially varying detector PSFs. Since collimated point source measurements are difficult to perform, as an initial validation of our approach we acquired line source data to estimate only the transverse detector blurring PSFs. The line sources were 0.3 mm inner diameter capillary tubes with 6 cm length. Two tubes were each filled with ~16 μCi of ^{18}F. The tubes were placed parallel to one another and 14 mm apart on a thin, stiff board. The two capillary tubes were oriented axially and positioned at 0 mm (tube 1) and 14 mm (tube 2) radial distance from FOV center. A total of 500,000 coincident events (2000 counts/sec x 5 minutes) were acquired. The tubes were stepped out radially in 2 mm increments until tube 1 overlapped the initial position of tube 2. Each acquisition was for a decay corrected, equivalent scan time. The data were collected in listmode format.

The detector ring was then manually rotated 10 degrees counter clockwise. Data were collected as the capillary tubes were stepped back toward the center of the detector ring between each measurement. By rotating the detector ring the bins associated with the gaps between adjacent detector modules were sampled.

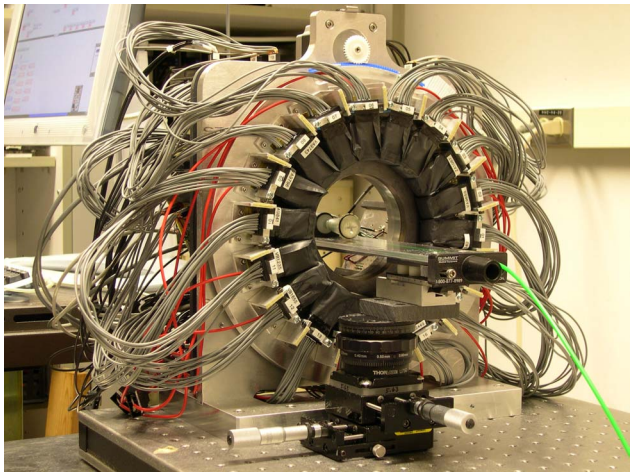

Figure 5. Single ring MiCES evaluation system (QuickPET II)

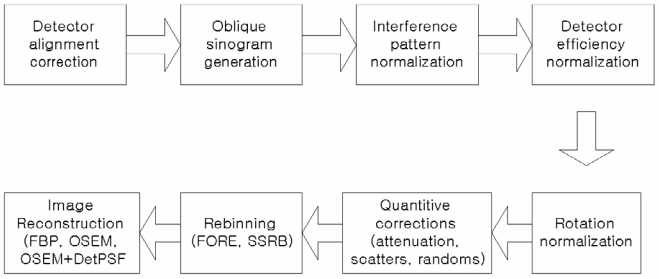

Figure 6. Block diagram of data acquisition from measured listmode data in QuickPET II.

The general procedure from collecting data through image reconstruction for the current MiCES evaluation system is illustrated in Fig. 6. Detector efficiency normalization and quantitative corrections are currently not implemented due to limitations of the current experimental environment.

Fig. 7 (a) shows the sinogram without alignment correction. The sinogram indicates significant distortion due to the misalignment of detector modules. Fig. 8 (b) illustrates alignment corrected sinogram, (c) sampling pattern normalized sinogram, and (d) gap compensated sinogram at (0,14) mm radial offset position.

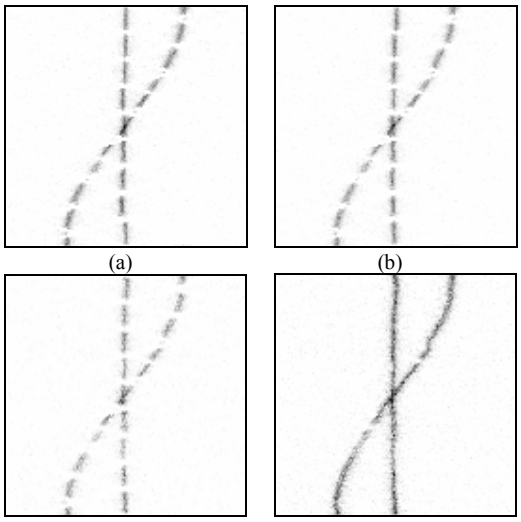

Figure 7. Intermediate sinograms through correction steps in Fig. 6. (a) before alignment correction, (b) after alignment correction, (c) after interference pattern normalization, (d) after rotation normalization

B. Parameterization of detector blurring PSF

After acquiring PSFs from line source sinograms, the PSFs were fitted with a weighted Gaussian-Lorentzian curve in (1).

$$f(x)=\begin{cases} a(we^{-\frac{(x-\mu)^2}{2\sigma_1^2}}+(1-w)\dfrac{1}{b_1(1+(\dfrac{x-\mu}{b_1})^2)}), x\le\mu \\ a(we^{-\frac{(x-\mu)^2}{2\sigma_2^2}}+(1-w)\dfrac{1}{b_2(1+(\dfrac{x-\mu}{b_2})^2)}), x>\mu \end{cases} \quad (1)$$

where w is a weight representing contribution of Gaussian term and μ is x value with respect to peak of $f(x)$. Since the PSFs are potentially asymmetric, the shape of function was divided into two halves centered on the peak value of x ($x=\mu$) and fitted with different Gaussian (σ_1, σ_2) and Lorentzian (b_1, b_2) half-width parameters, i.e. σ_1, b_1 for broader half toward FOV center and σ_2, b_2 for narrower half toward FOV boundary.

Fig. 8 illustrates the change of σ_1 and σ_2 parameters estimated from fitted curves from (0, 14) to (14, 28) mm off-centered positions. A least-squares fit to the measured data indicates that the asymmetric property becomes more significant as the distance from the FOV center increases. The same trend was recognized in the Lorentzian parameters (b_1, b_2) and the Gaussian weight w also varied with position.

Fig. 9 displays comparisons between sinogram PSFs acquired by measurements and those generated by parameterization at the center and 12 mm radial positions.

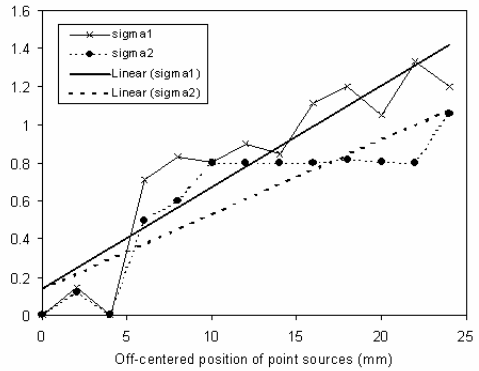

Figure 8. Estimated and least-squares fits to σ_1 and σ_2 in (1) as a function of radial distance from FOV center.

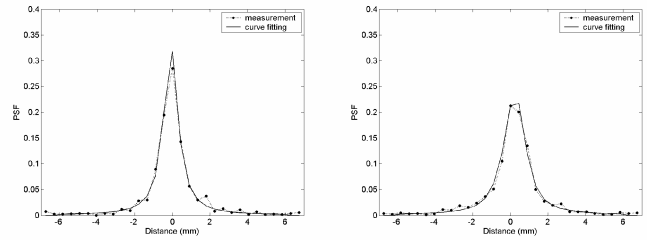

(a) PSFs at center (b) PSFs at 12mm offset

Figure 9. Experimental detector PSFs and corresponding fitted-curves.

C. Image reconstruction of real mouse measurements

The acquired detector PSFs were incorporated into the system model as described above to reconstruct real mouse images.

A p53 heterozygote female mouse on an NIH background with chemically induced skin tumors was imaged with FDG. The mouse was injected with 240 μCi of FDG via tail vein injection. Imaging began approximately one hour post-injection. To reduce uptake in the background tissues, the mouse was kept under light anesthesia (0.5-2.0% isoflurane) during radiopharmaceutical uptake. A 5 field of view scan was acquired over ~90 minutes. 21.3 million events were acquired during the study. Due to a handling error, the mouse was fed just before imaging and there was intense cardiac uptake as well as the expected tumor uptake.

Fig. 10 shows (a) transverse and (b) coronal sections of mouse images reconstructed with three different reconstruction techniques. The images on the left were reconstructed with FORE+FBP. The middle images used FORE+OSEM. As shown in the figure, the OSEM cleans up the image to some extent. The images on the right are results by FORE+OSEM incorporated with detector PSFs. Right images are much clearer and sharper than the others, which imply that the association of detector blurring PSFs within the system matrix can significantly improve image resolution.

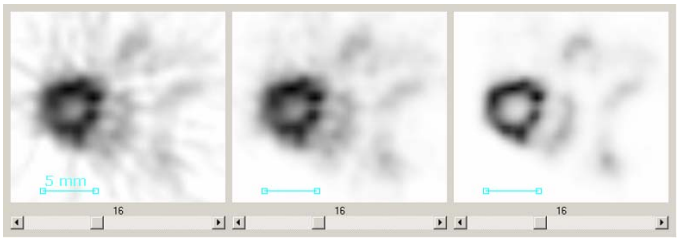

(a) Transverse slices

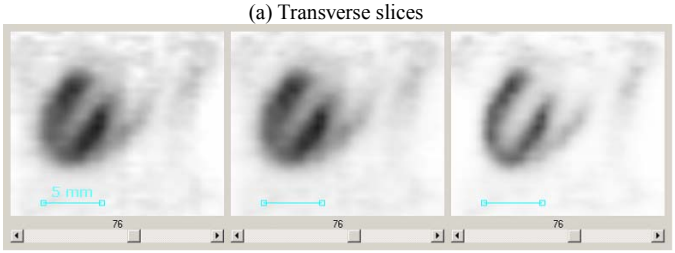

(b) Coronal slices

Figure 10. Mouse heart images in three different reconstruction method: FBP (left), OSEM (middle), OSEM with detector PSFs (right)

IV. Conclusion and Discussion

A pragmatic approach of image reconstruction was proposed for the fully-3D high resolution mouse imaging PET scanners. The proposed method is modeled on fully-3D image reconstruction used in clinical PET scanners, which is based on FORE rebinning followed by 2D OSEM iterative image reconstruction. In addition, we also used factorized system model incorporated with resolution sensitive physical effect in PET such as non-stationary detector blurring. This approach makes approximations that will reduce some measures of image quality as compared to those produced by a fully-Bayesian model of the acquisition process [8], [9]. The benifit, however, is decreased image reconstruction time. The relative merits of these two approaches, which will be the subject of further study, is a complex issue that depends on several factors including scanner design, choice of radioisotope, imaging task, and scanner throughput.

The proposed approach was applied to reconstruct images with data by simulation and measurement. In order to acquire simulation data, we used SimSET to model four ring MiCES mouse imaging scanner which is under development at the University of Washington while measured data was acquired from single-ring MiCES evaluation system called QuickPET II.

Reconstructions using the proposed method were presented from point source simulations and measured data from the QuickPET II system that were compared with images reconstructed by traditional methods in clinical imaging (FORE+FBP and FORE+OSEM). The results indicate that the proposed 'pragmatic' approach (FORE+OSEM incorporated with detector blurring PSFs) improved image resolution in terms of both contrast and FWHM without undue increases in noise.

Since the imaging study so far has been based on ^{18}F, the detector blurring effect is a more dominant effect on resolution recovery than positron range. Therefore positron range is not included in the current system model.

The factorized matrix for detector blurring PSFs used in this study was based on 1D blurring through the distance bin of projections without axial blurring component. Investigation of axial resolution recovery with 2D detector blurring matrix is also possible.

In addition, when noise measurement data is available, a quantitative study of the contrast versus noise trade-offs will be performed with the methods that we have previously used for simulation studies [3].

V. References

[1] R. S. Miyaoka, S. G. Kohlmyer, and T. K. Lewellen, "Performance Characteristics of Micro Crystal Element (MiCE) Detectors," *IEEE Trans. Nucl. Sci.*, vol. 48, no. 4, pp. 1403-1407, August 2001.

[2] M. Defrise, P. E. Kinahan, D. W. Townsend, C. Michel, M. Sibomana, and D. F. Newport, "Exact and Approximate Rebinning Algorithms for 3-D PET Data", *IEEE Transactions on Medical Imaging*, vol. 16, no. 2, pp. 145-158, April 1997.

[3] K. Lee, P. E. Kinahan, R. S. Miyaoka, J. Kim, and T K. Lewellen, "Impact of System Design Parameters on Image Figures of Merit for a Mouse PET Scanner," *IEEE Trans. Nucl. Sci.*, in press

[4] J. A. Fessler, "Aspire 3.0 User's Guide: A Sparse Iterative Reconstruction Library," Technical Report No. 293, Communications & Signal Processing Laboratory, University of Michigan, 2001

[5] J. A. Fessler, "Users Guide for Aspire 3D Image Reconstruction Software," Technical Report No. 310, Communications & Signal Processing Laboratory, University of Michigan, 2002

[6] J. A. Fessler, "Dynamic Libraries for ASPIRE Penalty Functions and System Models," Communications & Signal Processing Laboratory, University of Michigan, 2003

[7] X. Liu, C. Comtat, C. Michel, P. E. Kinahan, M. Defrise, and D. Townsend, "Comparison of 3-D Reconstruction With 3D-OSEM and With FORE+OSEM for PET," *IEEE Transactions on Medical Imaging*, vol. 20, no. 8, August 2001.

[8] J. Qi, R. M. Leahy, A. Chatziioannou, and T. H. Farquhar, "High-resolution 3D Bayesian Image Reconstruction Using the MicroPET Small-Animal Scanner," *Phys. Med. Biol.*, vol. 43, pp. 1001-1013, 1998

[9] R. M. Leahy and J. Qi, "Statistical Approaches in Quantitative Positron Emission Tomography", *Stat. Comp.*, vol.10, pp.147-165, 2000.

[10] S. Matej, J. S. Karp, R. M. Lewitt, and A. J. Becher, "Performance of the Fourier rebinning algorithm for PET with large acceptance angles," *Phys. Med. Biol.*, vol. 43, pp. 787-795, 1998.

[11] R. S. Miyaoka, M. L. Janes, B. K. Park, K Lee, P. E. Kinahan and T. K. Lewellen, "Toward the Development of a Micro Crystal Element Scanner (MiCES): quick PET II," IEEE NSS/MIC conference record, Portland, 2003.

[12] C. A. Johnson, Y. Yan, R. E. Carson, R. L. Martino, and M. E. Daube-Witherspoon, "A System for the 3D Reconstruction of Retracted-Septa PET Data Using the EM Algorithm", *IEEE Trans. Nucl. Sci.*, vol. 42, no. 4, pp.1223-1227, August 1995.

[13] E. U. Mumcuoglu, R. M. Leahy, S.R. Cherry, E. Hoffman, "Accurate Geometric and Physical Response Modelling for Statistical Image Reconstruction in High Resolution PET", *IEEE NSS/MIC*, vol. 3, pp. 1569-1573, November 1996.

[14] T. Frese, N. C. Rouze, C. A. Bouman, K. Sauer, and G. D. Hutchins, "Quantitative Comparison of FBP, EM, and Bayesian Reconstruction Algorithms for the IndyPET Scanner," *IEEE Transactions on Medical Imaging*, vol. 22, no. 2, February 2003.